ChemPlusChem

Research Article
doi.org/10.1002/cplu.202500243

Chemistry Europe
European Chemical Societies Publishing

www.chempluschem.org

Donor–Acceptor Interactions of $C_{60}F_{18}$ with Polycyclic Aromatic Hydrocarbons: Size Effects in Bulk Crystallization and Surface Constraints

Nicholas J. DeWeerd, Sebastian Balser, Long K. San, Rogger Palacios-Rivera, Steven H. Strauss, Esther Barrena, Yu-Sheng Chen, Carmen Ocal, Daniel Martin-Jimenez,* and Olga V. Boltalina*

An in-depth study of donor–acceptor (D/A) interactions between the high-dipole acceptor $C_{60}F_{18}$ (A) and polycyclic aromatic hydrocarbon (PAH) donors—pyrene, perylene, and coronene—reveals a surprisingly strong PAH size influence on the D/A complex stoichiometry and ordering in co-crystals. The crystallographic study shows the tendency of D/A mixtures to form stacked layered structures for the larger PAHs, perylene and coronene, while the role of aromatic π–π interactions diminishes, in contrast to the smaller pyrene/$C_{60}F_{18}$ system. The behavior of the layered-D/A assemblies is investigated by utilizing sequential deposition and co-evaporation of $C_{60}F_{18}$ and coronene on Au(111) surfaces. Scanning tunneling microscopy shows that the flat lying configuration adopted by coronene on the metal, which forms highly ordered close-packed monolayers stabilized by the interaction between their π electrons and the high density of gold surface states, hinders the formation of the ordered assemblies of the corresponding co-crystal. The influence of the substrate plus the critical role played by electronic and steric effects in the co-crystal formation are believed to cause the lack of viability. However, it is remarkable that, on the surface, adsorbed single $C_{60}F_{18}$ molecules are well centered on top of one coronene molecule, facilitating charge transfer between D and A molecules.

1. Introduction

Interactions between polycyclic aromatic hydrocarbons (PAHs) and 3D nanocarbons like fullerenes, have been extensively studied since pure fullerene-based materials have become available to researchers.[1] One of the earlier research areas focused on the photophysics of junctions formed by an electron donor and an electron acceptor material, with fullerenes used as acceptors, which resulted in the development of fullerene-based organic photovoltaics.[2,3] Furthermore, supramolecular chemistry involving "PAH host/fullerene guest" systems has enabled effective fullerene separation techniques and the development of molecular recognition strategies. This includes development of highly efficient chromatographic techniques, which utilize the propensity of π-systems of different fullerenes to strongly interact with π-systems of PAHs bonded to stationary phases, including pyrenylpropyl and phenathiazinyl-bonded silica.[4,5] PAH-based organic semiconductors, such as acenes, thiophenes, and aza-PAHs were successfully doped with strong fullerene acceptors, such as polyfluorofullerenes, resulting in improved performance of organic thin film transistors, organic light emitting devices, and photovoltaics.[6,7] The impact of charge transfer between organic polyaromatic semiconductors and *p*-dopants on the optoelectronic properties has recently become an active research area, highlighting the need for a deeper molecular-level understanding of the nature of intermolecular interactions between electron donor (D) and acceptor (A) molecules.[8] In particular, charge-transfer interactions in D/A co-crystals is an important area of study for the development of new optoelectronic functionalities, with an urgent demand to reveal structure–property relationships.[9–11]

This work reports the first systematic study of a series of D/A complexes of various PAH donor molecules with the fluorofullerene acceptor $C_{60}F_{18}$ (see **Figure 1**) using single-crystal X-ray diffraction (XRD) and UV-vis spectroscopy. We also present a scanning tunneling microscopy (STM) study for the particular case of $C_{60}F_{18}$ and coronene on a metal surface.

N. J. DeWeerd, S. Balser, L. K. San, S. H. Strauss, O. V. Boltalina
Department of Chemistry
Colorado State University
Fort Collins, CO 80523, USA
E-mail: olga.boltalina@colostate.edu

R. Palacios-Rivera, E. Barrena, C. Ocal, D. Martin-Jimenez
Institute of Materials Science of Barcelona (ICMAB-CSIC)
Bellaterra, 08193 Barcelona, Spain
E-mail: daniel.martin@csic.es

Y.-S. Chen
ChemMatCARS
University of Chicago Advanced Photon Source
Argonne, IL 60439, USA

Supporting information for this article is available on the WWW under https://doi.org/10.1002/cplu.202500243

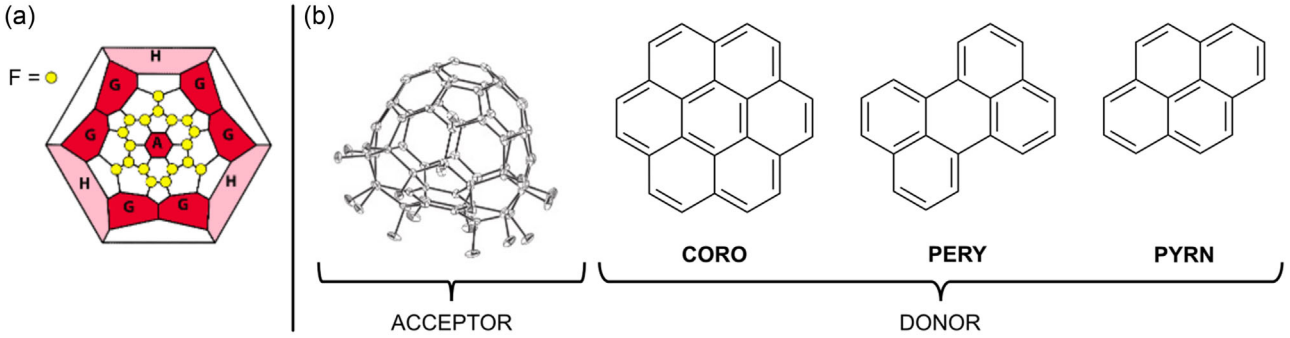

Figure 1. a) Schlegel diagram of $C_{60}F_{18}$, showing, qualitatively, the gradient shading of hexagons according to their nucleus-independent chemical shift (NICS) values: red for hexagons A (NICS = −14.3) and G (NICS = −12.1), pink for H hexagons (NICS = −11.5).[15] The positions of the 18 C(sp^3) atoms that bear the F atoms are indicated by yellow circles. b) Schematic molecular structure of the $C_{60}F_{18}$ acceptor (from X-ray data in this work) and the drawings of donors coronene (CORO), perylene (PERY), and pyrene (PYRN) used in this work.

2. Results and Discussion

2.1. X-ray Crystallographic Study of Donor–Acceptor Complexes of $C_{60}F_{2n}$ with PAHs

Among many reported fluorofullerenes $C_{60}F_{2n}$, where $2n = 0$–20, 36, 48, the choice of $C_{60}F_{18}$ as an acceptor was based on the following. First, it is a good electron acceptor, with an estimated gas-phase electron affinity (EA_g) value of 3.1–3.3 eV, nearly 0.5 eV higher than that of the non-fluorinated parent C_{60}, but ≈0.7 and 1.0 eV lower than highly fluorinated counterparts $C_{60}F_{36}$ and $C_{60}F_{48}$, respectively.[12] Second, it has a unique molecular structure that is composed of two hemispheres: a fluorinated one, where the 18 F atoms are attached to a loop of 15 contiguous C(sp^3) atoms surrounding an isolated A-type hexagon of C(sp^2) atoms, plus to 3 C(sp^3) atoms that radiate symmetrically from the loop, and a C_{60}-like bare hemisphere (see Figure 1a). As a consequence, the molecule has a very high-dipole moment of 13.3 D,[13] a large gradient of electrostatic potential and strong electron acceptor properties.[14] The presence of the belt of 18 F atoms significantly affects the local aromaticity of the polygons on the cage, such that the nucleus-independent chemical shift (NICS) values range widely from −10 to −14 (cf. C_{60} NICS = −6.8), as calculated in ref. [15] by the Hartree–Fock method; three types of hexagons with the highest local aromaticity are highlighted in red and pink in Figure 1a, with their NICS values given in the caption of Figure 1. These hexagon notations will be used below for descriptions of specific intermolecular interactions of $C_{60}F_{18}$ with PAH donors.

The described structural and electronic features make $C_{60}F_{18}$ a particularly interesting model compound for studies of intermolecular π–π interactions with polyaromatic molecules in the crystalline phase and on surfaces. In higher fluorinated homologs, such as $C_{60}F_{48}$ and $C_{60}F_{36}$, the π-systems (isolated hexagons or double bonds) are shielded by evenly distributed F atoms on the cage, preventing close contact with other polyaromatic molecules.[16] In $C_{60}F_{18}$, in contrast, the bare carbon hemisphere is sterically and electronically accessible for close contacts with electron-rich conjugated donor molecules.

Three PAHs were selected as donor compounds: pyrene (PYRN), perylene (PERY), and coronene (CORO) (see Figure 1b for schematic molecular drawings). They have different sizes (composed of four, five, and seven cycles, respectively) and shapes, and their first ionization energies differ, ranging from 6.96 eV (PERY),[17] to 7.26 eV (CORO),[17] to 7.426 eV (PYRN)[18] allowing one to probe electronic and steric effects in the interaction with the acceptor. All three are commonly used as building blocks for high-performance organic semiconductors, supramolecular assembling of two-dimensional (2D) structures or the synthesis of large and well-defined 2D nanographene molecules.[19,20]

Co-crystals were formed from solution for X-ray crystallographic studies. We avoided the use of aromatic solvents as they are known to have a tendency to form crystalline solvates with fluorofullerenes.[13,21] Co-crystals were grown by slow evaporation of dichloromethane solutions containing a 1:1 molar ratio of the donor (D) and acceptor (A) molecules. XRD data collection and final refinement parameters for the co-crystal structures are listed in **Table 1**.

Dichloromethane solutions of all PAHs, except perylene, were colorless, whereas the $C_{60}F_{18}$ solution was pale yellow. Upon mixing, darker-yellow to red solutions formed, indicative of charge-transfer (CT) complex formation, with UV-vis absorption spectra for PYRN/$C_{60}F_{18}$ and CORO/$C_{60}F_{18}$ solutions showing weak charge-transfer bands at λ_{max} 490–515 and 500–515 nm, respectively (see Figure S1, Supporting Information). Attempts to record the UV-vis spectrum of the charge-transfer complex PERY/$C_{60}F_{18}$, were made but, apparently due to the sparing solubility of the charge-transfer complex in dichloromethane, the CT band was not detected during these experiments. In the solid state the charge-transfer interaction between the PAHs and $C_{60}F_{18}$ is evidenced by the color of the crystals which were red, green, and purple for the CORO, PERY, and PYRN co-crystals, respectively. In addition to $C_{60}F_{18}$, other fluorofullerenes with 36 and 48 F atoms were also used to attempt co-crystallization with the selected donor compounds, but neither $C_{60}F_{36}$ nor $C_{60}F_{48}$ formed co-crystals suitable for single-crystal XRD. Upon mixing the $C_{60}F_{36}$ and $C_{60}F_{48}$ solutions with the dissolved donors, intense dark red solutions were formed indicating CT complex formation, in agreement with their stronger acceptor properties.[22] The failure to form high-quality co-crystals for XRD data acquisition may be due to the disorder of these highly substituted higher-symmetry fluorofullerenes and an absence of

Table 1. X-ray diffraction data collection and final refinement parameters for $(PYRN)_2/C_{60}F_{18}{\cdot}CH_2Cl_2$, CORO/$(C_{60}F_{18})_2$, and PERY/$C_{60}F_{18}$.[a)]

Compound	$(PYRN)_2/C_{60}F_{18}/CH_2Cl_2$	CORO/$(C_{60}F_{18})_2$	PERY/$C_{60}F_{18}$
Empirical formula	$C_{93}H_{22}F_{18}Cl_2$	$C_{144}H_{12}F_{36}$	$C_{80}H_{12}F_{18}$
Molecular wt., [g mol^{-1}]	1552.01	2425.54	1314.90
Habit, color	Needle, purple	Plate, red	Plate, dark green
Space group, *Z*	$P2_12_12_1$, 4	$P2_1/c$, 4	*Pnma*, 4
a, Å	13.3741(8)	44.872(4)	11.4988(8)
b, Å	19.5758(12)	11.1086(9)	23.8011(16)
c, Å	22.2815(12)	17.4423(15)	17.1844(11)
α, deg	90	90	90
β, deg	90	96.759(2)	90
γ, deg	90	90	90
V, $Å^3$	5833.5(6)	8633.9(13)	4703.1(5)
T, K	100	100	150
ρ_{calc}, g cm−3	1.767	1.866	1.857
$R(F)$ $(I > 2\sigma(I))$[b)]	0.0338	0.0960	0.0535
$wR(F^2)$ [all data][b)]	0.0857	0.2552	0.1713
GooF	1.027	1.058	0.991
C—C bond precision, Å	0.0040	0.0085	0.0025
CCDC deposition #	2433853	2433669	2433283

[a)]PYRN = pyrene; CORO = coronene; PERY = perylene. [b)]$R(F) = \Sigma||F_o| - |F_c||/\Sigma|F_o|$; $wR(F^2) = (\Sigma[w(F_o{}^2 - F_c{}^2)^2/\Sigma[w(F_o{}^2)^2])^{1/2}$.

preferential and accessible sites for π–π interactions with the PAH donors that were used.

2.2. The Structure of $(PYRN)_2/C_{60}F_{18}{\cdot}CH_2C_{l2}$

The co-crystal has a 2:1 (D:A) stoichiometry. Relevant portions of the $(PYRN)_2/C_{60}F_{18}{\cdot}CH_2Cl_2$ structure are shown in **Figure 2**. The complete structure based on the XRD data and the thermal ellipsoid plot of $(PYRN)_2/C_{60}F_{18}{\cdot}CH_2Cl_2$ are displayed in Figure S2 and S3 (Supporting Information). Figure 2a shows a $C_{60}F_{18}$ molecule and the three PYRN molecules to which it shares significant π–π overlap (the yellow spheres are F atoms). The three fullerene hexagons that exhibit π–π overlap with three PYRN molecules are highlighted in red or pink. Note: while three closest PYRN molecules are shown in Figure 2a, only two belong in the smallest repeating unit of the structure. See Figure S3, Supporting Information for the smallest repeating unit as well as Figure S2, Supporting Information for depictions of the complex packing, which leads to close interactions between multiple molecules. These fullerene hexagons, labeled G (red) or H (pink), are also indicated in the $C_{60}F_{18}$ Schlegel diagram shown in Figure 2b, (the C atoms to which the 18 F atoms are attached are highlighted in yellow). Notably, the G hexagons and H hexagon have high local aromaticity on the cage (NICS = −12.1 and −11.5, respectively). The unique $C(sp^2)_6$ hexagon, A (defined in Figure 1) connected to six $C(sp^3)$–F vertexes, has the highest local aromaticity (NICS = −14) but is too sterically hindered for close π–π interactions.

Figure 2c shows the G (red, $C(sp^2)$ atoms) or H (pink, $C(sp^2)$ atoms) fullerene hexagons and their π–π overlapped PYRN molecules. The least-squares planes of the virtually planar PYRN molecules are in the plane of the page. The least-squares planes of three fullerene hexagons are tilted from the plane of the page by (left to right) 10.5, 0.0, and 10.0°. The perpendicular distances of the fullerene hexagon $C(sp^2)$ atoms from their respective PYRN least-squares planes are (left to right) 3.16–3.66, 3.26–3.34, and 3.10–3.56 Å. There are no PYRN–PYRN π–π overlaps.

As revealed in this structural analysis, such strong π–π interactions between multiple PYRN molecules and a $C_{60}F_{18}$ molecule may shed light on the previous success in isolation of this and other fluorofullerenes from reaction mixtures.[14,23,24] The chromatographic method employed a column with a PYRN-modified stationary phase (COSMOSIL Buckyprep, Nacalai Tesque, Japan) for separation of the fluorofullerene mixtures containing $C_{60}F_{2n}$, where $2n = 0$–20, and 36. The high-performance liquid chromatography (HPLC) retention time of $C_{60}F_{18}$ ($t_R = 38$ min) is much longer than the retention times of C_{60} ($t_R = 8$ min) and $C_{60}F_{36}$ ($t_R = 3.1$ min).[23] The specific strong interaction of multiple stationary-phase pyrene moieties with fullerenes that have fewer than 20 electron-withdrawing Cl, CF_3, or R_F groups has played a pivotal role in the isolation of dozens of fullerenes with diverse structures and unique properties,[25] including the record-breaking 27 positional isomers of $C_{60}(CF_3)_{10}$[26] and 48 isomers of $C_{70}F_{38}$.[27] Notably, conventional chromatographic C18 columns have failed to provide effective separations of such materials because of the lack of specific π–π interactions between the fullerenes and the stationary phase.

2.3. The Structure of $PERY/C_{60}F_{18}$

The co-crystal has a 1:1 D/A stoichiometry. Some drawings illustrating the X-ray crystal structure are shown in **Figure 3** and S4, S5, Supporting Information. Both molecules are located on special positions: the PERY donor on an inversion center and the $C_{60}F_{18}$ acceptor on a two-fold axis parallel to the crystallographic *a* axis. The structure consists of alternating close-packed layers of $C_{60}F_{18}$ molecules and close-packed layers of PERY molecules, as shown in Figure 3b. The close-packed layers are shown in Figure 3c and are parallel to the crystallographic *ac* plane and are stacked along the crystallographic *b* axis. The distances between $C_{60}F_{18}$ centroids (i.e., the centroids of the 60 C atoms) in the close-packed planes are 9.848 (×2), 10.839 (×2), and 11.499 (×2) Å. The distances between PERY centroids (the centroids of the 20 $C(sp^2)$ PERY atoms) are 10.338 (×4) and 11.499 (×2) Å. The centroids in the $C_{60}F_{18}$ layers are rigorously co-planar, as are the centroids in the PERY layers, and the least-squares planes of the two types of centroid layers are rigorously parallel to the *ac* plane. The perpendicular distance between the planes is 5.950 Å.

The vector defined by centroids of the C_{60} cage and the hexagon A (i.e., the electric dipole vector) is tilted 69° from the

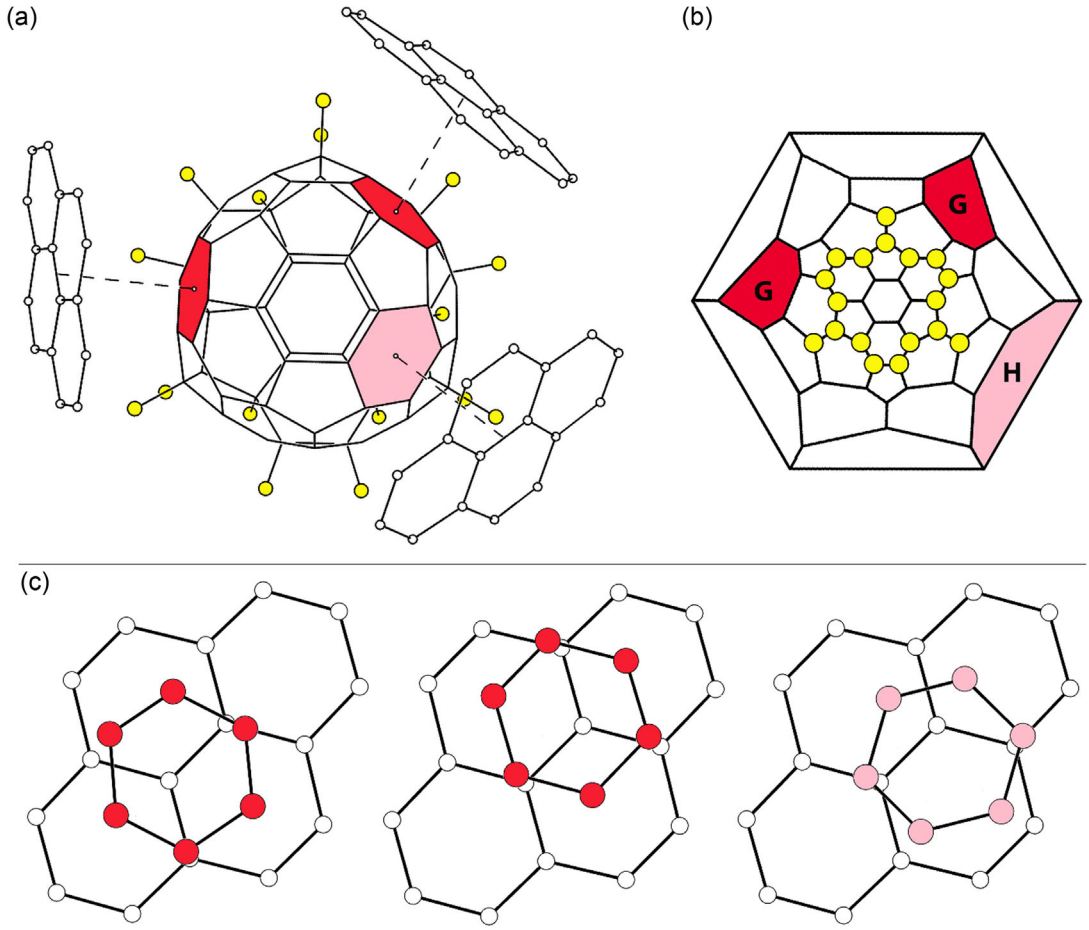

Figure 2. a) Portions of the X-ray structure of $(PYRN)_2/C_{60}F_{18}{\cdot}CH_2Cl_2$ (the PYRN H atoms and the CH_2Cl_2 solvent molecule were omitted for clarity) and b) the Schlegel diagram of $C_{60}F_{18}$ with highlighted red and pink hexagons that have the closest π–π overlap with three different PYRN molecules shown in (c). See text for details and Supporting Information (Figure S2 and S3, Supporting Information).

plane of the C_{60} centroids, with the tilt toward the nearest-neighbor direction of the $C_{60}F_{18}$ close-packing.

The PERY molecules are "sandwiched" between two $C_{60}F_{18}$ molecules in two planes, as shown Figure 3a, and make close approaches to a $C_{60}F_{18}$ hexagon G, highlighted in red, in each of those two $C_{60}F_{18}$ molecules.

A parallel exists between this structure and the structure of the hexamethylbenzene (HMB) solvate of $C_{60}F_{18}$.[28] In the latter, planes of $C_{60}F_{18}$ molecules and planes of HMB molecules are arranged parallel to the crystallographic *ab* plane. The planes are stacked in the direction of the crystallographic *c* axis in the orthorhombic unit cell, and the planes of the molecules are 5.45 Å apart.[28]

2.4. The Structure of CORO/$(C_{60}F_{18})_2$

Some drawings illustrating the structure obtained from X-ray data are shown in **Figure 4**, **5** and S6–S8, Supporting Information. The co-crystals have a 1:2 D/A stoichiometry. Layers of CORO molecules are separated by a double layer of $C_{60}F_{18}$ molecules. The layers are parallel to the crystallographic *bc* plane and are stacked along the *a*-axis. The CORO centroid planes and $C_{60}F_{18}$ centroids planes are rigorously parallel. The perpendicular distance between adjacent planes of CORO and $C_{60}F_{18}$ molecules is 6.486 Å. The CORO molecule is located on a crystallographic inversion center, so only half of the coronene molecule is unique.

The CORO centroid–centroid distances are 10.325 (×4) and 11.093 (×2) Å. The average CORO centroid–centroid distance is 10.581 Å, which is nearly the same as the 10.645 Å average centroid–centroid distance between the $C_{60}F_{18}$ molecules in the close-packed layers in that structure. The geometric constraint of the lattice requires that the area of the hexagonal array of CORO centroids must be equal to the area of the hexagonal array of $C_{60}F_{18}$ centroids. Thus, the CORO molecules are tilted with respect to the plane of their centroids by 21.8°. The dihedral angles between the planes of adjacent CORO molecules are either 0.00° or 27.2°.

The structure of solvent-free $C_{60}F_{18}$ was first published by Goldt, Boltalina, et al. in 2002.[26] A much higher resolution structure was published in the 2007 charge-density paper by Hübschle, Luger, Boltalina, et al.[27] The space group is Cc, which is non-centrosymmetric. Therefore, crystals of solvent-free $C_{60}F_{18}$ are polar, though this was not discussed in any of these papers. The comparison of the in-plane packing of $C_{60}F_{18}$ in CORO/$(C_{60}F_{18})_2$ and solvent-free $C_{60}F_{18}$ is presented in Figure S6,

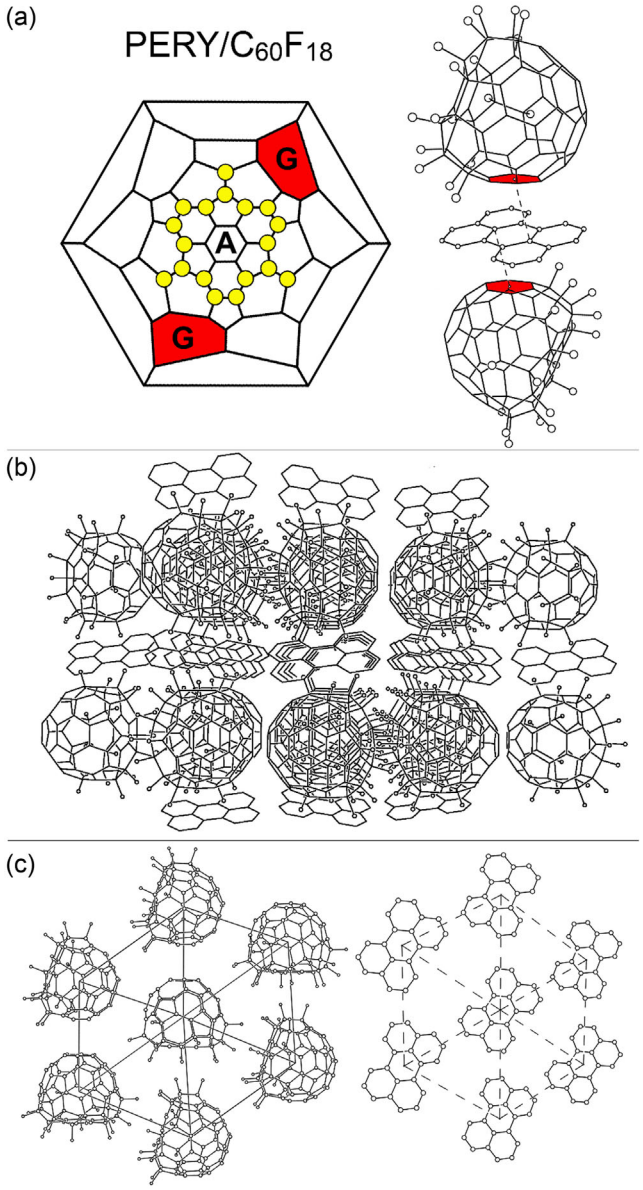

Figure 3. a–c) Relevant portions of the structure of PERY/$C_{60}F_{18}$ and a) a Schlegel diagram of $C_{60}F_{18}$ with red G hexagons that have close π–π overlap with PERY molecules. See text for details and Supporting Information (Figure S4 and S5, Supporting Information). The layers are in the crystallographic ac planes and are stacked along the b axis.

Supporting Information. The $C_{60}F_{18}$ molecules in the solvent-free structure are not as closely packed (average centroid–centroid distance = 11.115 Å) as in the planes of fullerenes in the structure of CORO/$(C_{60}F_{18})_2$ (average centroid–centroid distance = 10.655 Å). However, in the perpendicular direction (see Figure S7, Supporting Information), the packing is slightly more compact for the solvent-free structure: the distance between planes of $C_{60}F_{18}$ molecules in the solvent-free $C_{60}F_{18}$ structure is 8.276 Å whereas it is 9.278 Å in the CORO/$(C_{60}F_{18})_2$ co-crystal. This difference in the interlayer spacing is clearly a result of the different orientations of the molecules with respect to the close-packed planes for each structure. In solvent-free $C_{60}F_{18}$, the benzenoid hexagon is tilted 29.4° from the plane of the $C_{60}F_{18}$ centroids, allowing the layers to approach more closely than in CORO/$(C_{60}F_{18})_2$, in which the fullerene benzenoid hexagon is nearly perpendicular to the close-packed layer (the tilt angle is 88.4°). In solvent-free $C_{60}F_{18}$, the fullerene dipoles are all oriented in the same direction, resulting in the formation of polar crystals. The same is true for each double layer of $C_{60}F_{18}$ molecules in CORO/$(C_{60}F_{18})_2$. However, in the co-crystal structure the dipoles in successive double layers are oriented in opposite directions (see Figure 5c).

Notably, upon increasing the size of the planar PAH donor in co-crystals with $C_{60}F_{18}$, the molecular ordering changes significantly. In contrast to the complex array in the structure of $(PYRN)_2/C_{60}F_{18}{\cdot}CH_2Cl_2$, where each $C_{60}F_{18}$ is surrounded by three PYRN molecules with π–π overlap distances of 3.3–3.4 Å, the PERY and CORO with $C_{60}F_{18}$ resulted in stacked layered co-crystal structures with close-packed planes of PAH or $C_{60}F_{18}$ molecules. In the case of PERY, an alternate stacking of donor and acceptor molecular planes was found (i.e., D/A/D/A) whereas in the case of CORO a D/A/A/D/A/A stacking was observed, with no aromatic π–π overlap between the CORO donor and the $C_{60}F_{18}$ acceptor, but with a remarkable polar orientation of the $C_{60}F_{18}$ molecules with respect to the plane formed by the CORO molecules. This observation led us to explore the interface between donor and acceptor on a Au(111) surface, despite the low charge transfer expected in this system (see above). Two cases were investigated by means of STM, the sequential deposition of $C_{60}F_{18}$ onto an already formed CORO monolayer and co-deposition of both molecules.

2.5. STM Study of $C_{60}F_{18}$ and CORO on Au(111)

We performed an STM study in ultrahigh vacuum (UHV) ($p \approx 10^{-10}$ mbar) on Au(111), as it is chemically inert and has a well-defined, atomically flat surface presenting the well-described $(22 \times \sqrt{3})$ surface reconstruction, also known as herring bone (HB), that is ideal for high-resolution STM imaging.[28–33] Interestingly, the well-known HB superstructure will serve as in-situ reference for in-plane crystallographic determination. In addition to being a reasonable choice for the bottom-up growth of D/A architectures, CORO was selected out of the three investigated PAHs due its well-documented two-dimensional (2D) ordered assembly on the Au(111) surface.[29,32] To avoid the incorporation of solvent molecules, $C_{60}F_{18}$ and CORO were deposited by sublimation onto the HB reconstructed Au(111) surface maintained at room temperature (RT) in UHV during molecular deposition. Before discussing our approach for achieving the on-surface donor and acceptor interface (D/A or A/D), we first address the separate assembly of $C_{60}F_{18}$ and CORO directly on the surface. All STM images presented were taken at RT in the constant current operation mode (I = cte). In this mode, topographic images correspond to the density of states (DOS) contour of the surface at a given tip-sample bias voltage (U).

Figure 6 displays STM images after the formation of a CORO monolayer. As observed in all images, the molecules assemble into a long-range highly ordered closed-packed hexagonal arrangement, with an intermolecular distance of (11.5 ± 0.8) Å. The hexagonal unit cell aligns with the $[1\bar{1}0]$ direction of the gold surface (nearest-neighbor or NN direction). The steps and HB reconstruction of the Au(111) substrate remain unaltered beneath

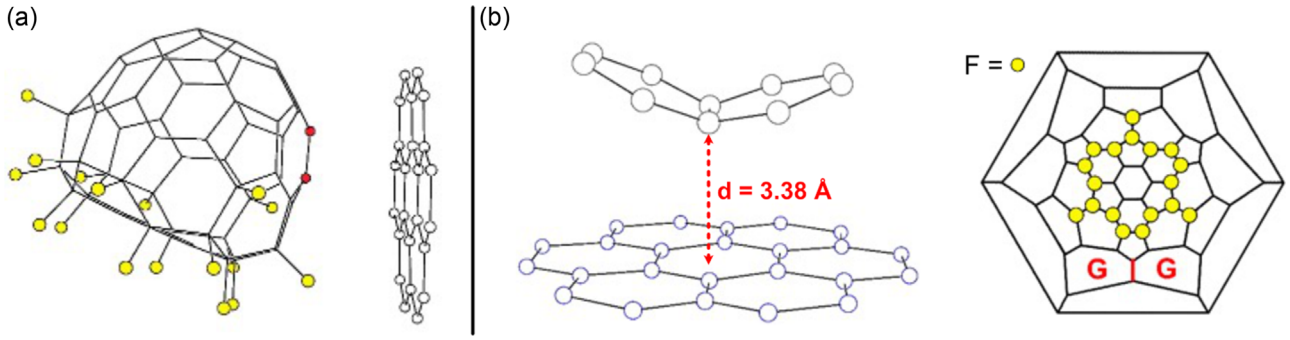

Figure 4. Detail of the structure of CORO/$(C_{60}F_{18})_2$ shown in Figure 5. a) The closest C(sp^2)—C(sp^2) bond of $C_{60}F_{18}$ (an edge common to two G hexagons) is highlighted in red and F atoms are colored in yellow. b) Portion of the structure showing the closest distance between the CORO centroid and the edge common to the two G hexagons of $C_{60}F_{18}$. The yellow circles in the Schlegel diagram show the positions of the 18 C(sp^3) atoms bearing the F atoms. Thermal ellipsoid plot of the structure is given in Figure S8, Supporting Information.

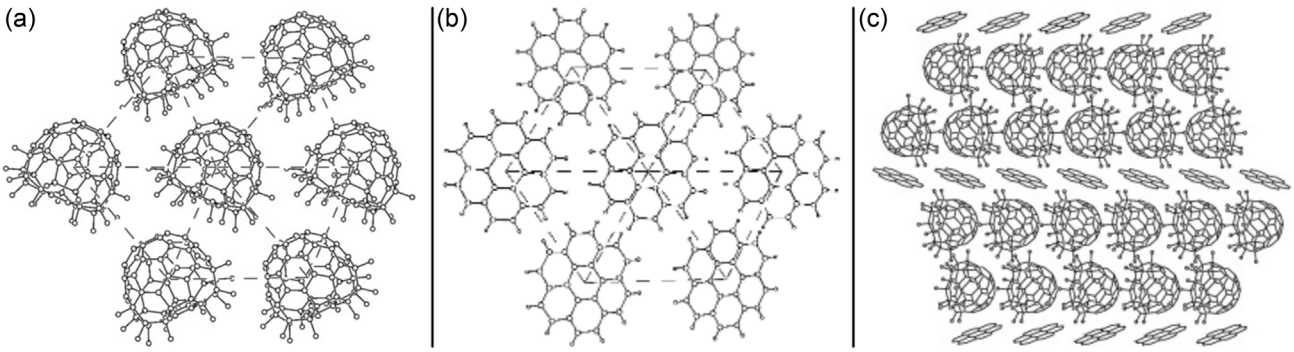

Figure 5. Top views of $C_{60}F_{18}$ a) and CORO b) layers, respectively, in the structure of CORO/$(C_{60}F_{18})_2$. The $C_{60}F_{18}$ centroid–centroid distances are 9.534 (×2), 11.093 (×2), and 11.307 (×2) Å. The CORO centroid–centroid distances are 10.332 (×4) and 11.093 (×2) Å, which are similar to the PERY centroid–centroid distances in the structure of PERY/$C_{60}F_{18}$ (see Figure 3). c) Side view of the stacking of layers of CORO molecules and double layers of $C_{60}F_{18}$ molecules. The layers are parallel to the crystallographic bc plane and are stacked along the a-axis.

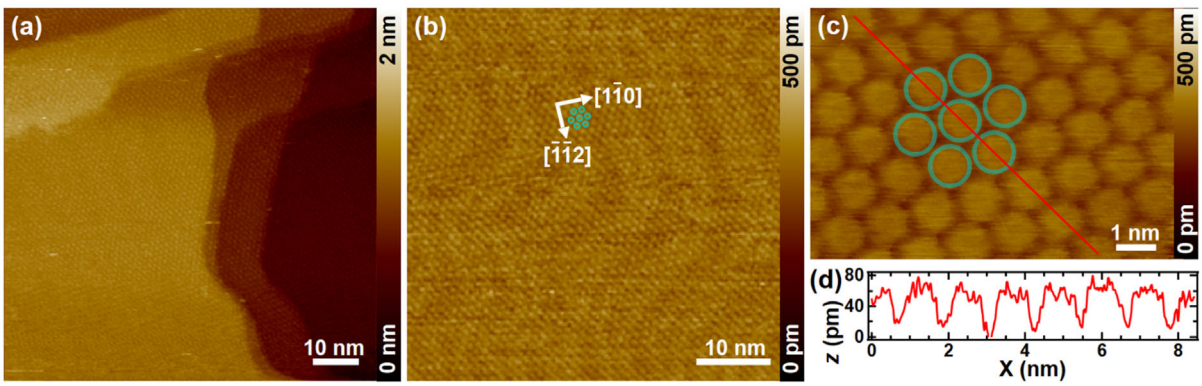

Figure 6. STM topographic images of a CORO monolayer on Au(111). In the larger images, a,b), diverse steps and the characteristic herringbone (HB) structure of the underlying Au(111) are visible. The near-neighbor (NN) and next-near-neighbor (NNN) directions of the (111) substrate are indicated in (b) by [1$\bar{1}$0] and [$\bar{1}\bar{1}$2], respectively. The green circles in b,c) correspond to the hexagonal packing of CORO with a distance of 11.5 ± 0.8 Å between the molecules' centroids. d) Height profile along the red line in panel c). STM parameters: $U = 1.5$ V and $I = 4$ nA.

the carpet-like molecular layer and is perfectly visible in the large-scale STM image (see Figure 6a,b), indicating a moderate interaction of the molecules with the gold surface. From the high-resolution image in Figure 6c it is also inferred that CORO adsorbs planarly (i.e., aromatic rings parallel to the surface plane) onto Au(111). Figure 6d displays a cross-section, along the red line in Figure 6c, quantitatively providing the periodicity and low corrugation of the molecular arrangement. Overall, we observe that CORO forms a flat monolayer in full agreement with the reported (4 × 4) epitaxial structure on Au(111),[30–32] that is, the distance between CORO molecules is 4 times the Au lattice constant (2.89 Å). Similarly to the individual CORO layers in the CORO/$(C_{60}F_{18})_2$ structure, the CORO monolayer on Au(111) exhibits a hexagonal packing. The difference in the intermolecular centroid distance, or difference

in the in-plane periodicity, is less than 12% between the two structures, being due to the out-of-plane molecular tilt of CORO in the co-crystal (Figure 5c).

Figure 7 displays representative topographic images obtained after a submonolayer coverage of $C_{60}F_{18}$ on Au(111) (below ≈50% of monolayer completion) at RT. We observe that $C_{60}F_{18}$ does not present long-range order over the surface but forms 2D irregular islands that coexist with small aggregates a few nanometers in diameter, indicated by blue arrows in Figure 7b (upper inset in Figure 7b as illustration depicting an $C_{60}F_{18}$ aggregate). Notably, longer evaporation times led to the formation of larger disordered aggregates, making STM imaging more difficult or even impossible. As can be seen in the large-scale Figure 7a, the molecular assembly consists of islands with irregular shape and a large variability in size. Outstandingly, despite no long-range order being observed, a clear short-range order is seen in the lower-scale images in Figure 7b,c. The $C_{60}F_{18}$ molecules are arranged in what seems to be a defective hexagonal packing, with an average intermolecular distance of (11 ± 1) Å and an apparent height between 400 and 500 pm (see Figure 7d and S9, Supporting Information). As already reported for distinct fluorinated fullerenes on surfaces,[34–36] irregular islands' shape, clustering and inhomogeneous DOS contours are typical consequences derived from a limited surface diffusion at RT. Note that DOS will depend on the amount of F atoms exposed at each molecule and that the symmetry breaking induced by fluorination leads to an increase of the possible molecular orientations on the surface (see the scheme in the lower inset of Figure 7b depicting this circumstance). This fact implies a complex scenario, in which dipole–dipole interactions are a key factor for the assembly of non-symmetric $C_{60}F_{18}$ on surfaces. For comparison, the simplest case of C_{60} on Au(111) is presented in Figure S10, Supporting Information. Therefore, for achieving a good interface between donor and acceptor, the growth of an ordered and close-packed 2D assembly of $C_{60}F_{18}$ on Au(111) proves to be non-trivial.[37] Conversely, as demonstrated above, a complete monolayer of CORO, with an extended long-range order and homogeneous 2D structure, seems to be a suitable template for obtaining an A/D architecture on Au(111).

To access the interface between CORO and $C_{60}F_{18}$ molecules, by taking advantage of a high quality and ordered template, **Figure 8** exemplifies what is obtained upon deposition of $C_{60}F_{18}$

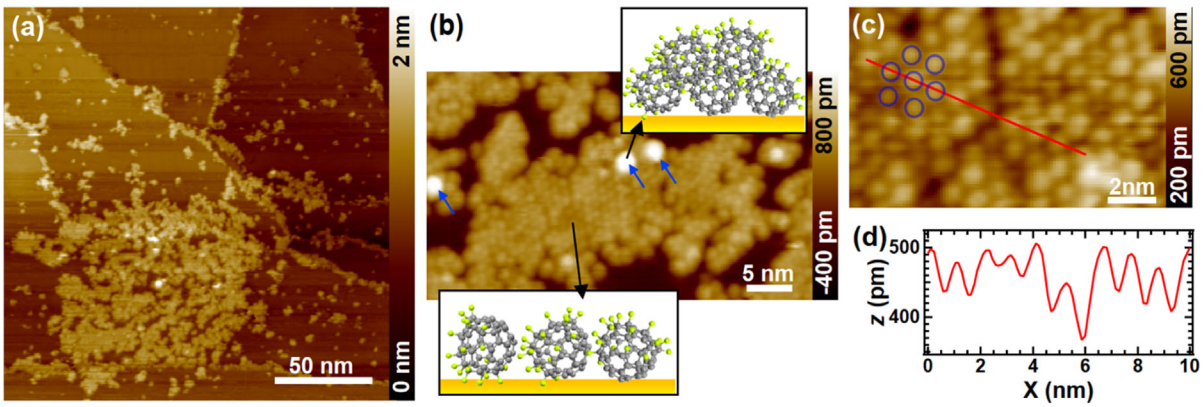

Figure 7. a,b) STM topographic images of islands of $C_{60}F_{18}$ on Au(111) ($U = 2.1$ V and $I = 76$ pA). Blue arrows in b) indicate small $C_{60}F_{18}$ aggregates. The upper and lower insets in (b) shows respectively schemes depicting a $C_{60}F_{18}$ aggregate and a monolayer of $C_{60}F_{18}$ with different orientations. c) STM topographic image of islands of $C_{60}F_{18}$ on Au(111) ($U = 1.9$ V and $I = 55$ pA). Blue circles indicate the hexagonal packing of $C_{60}F_{18}$ with an intermolecular distance of 11 ± 1 Å. d) Cross-section along the red line in (c).

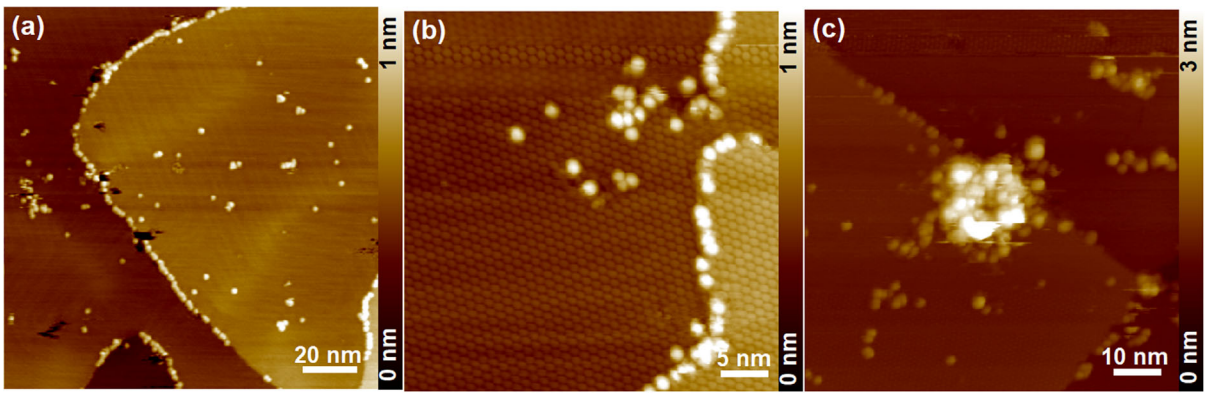

Figure 8. STM topographic images of a very low amount of $C_{60}F_{18}$ deposited on a complete CORO monolayer formed on Au(111). STM parameters are: a) $U = 0.7$ V and $I = 220$ pA, b) $U = 1.4$ V and $I = 600$ pA and c) $U = 2$ V and $I = 150$ pA. Details on the adsorption site of $C_{60}F_{18}$ relative to the HB of Au(111) and $C_{60}F_{18}$ clusters are provided in Figure S11, Supporting Information.

(with the same exposure as for Figure 7) onto the previously prepared CORO monolayer that uniformly covers the reconstructed Au(111) substrate. The first noticeable observation when comparing Figure 6a and 8a is a preferential nucleation of $C_{60}F_{18}$ at the step edges. On the terraces, either isolated molecules or small clusters with a few molecules of $C_{60}F_{18}$ are observed (more details in Figure S11, Supporting Information). In some regions, the formation of large 3D aggregates posed difficulties for STM imaging (see Figure 8c).

Importantly, isolated single $C_{60}F_{18}$ molecules could be imaged to get insight about the A/D system at the molecular level. As shown in **Figure 9**, high-resolution constant current (topography) STM combined with frequency-modulated atomic force microscopy allowed the determination of the preferential adsorption site of the fluorinated fullerene on the CORO layer. The $C_{60}F_{18}$ molecules appear with a similar apparent height to that obtained on Au(111) (see the height profile in the inset of Figure 9a). Note that in the frequency shift channel (see Figure 9b) the molecules appear darker (inverse contrast than in the topographic image). It can be observed that a single $C_{60}F_{18}$ molecule sits at the center of the hexagonal lattice defined by the underlying CORO molecules, indicating that the fullerene adsorbs on a "top" position, the central ring of one CORO molecule. To help visualization, the hexagonal lattice of the CORO monolayer has been superimposed in the inset of Figure 9b. Though the relative position of the molecules differs from that on the reported co-crystal (see Figure 5c), these results provide evidence of a dominant $C_{60}F_{18}$-CORO interaction suitable to form a D/A complex. The larger interaction (darker color in the frequency shift image) on top of the donor–acceptor pair might respond to a certain substrate-mediated charge transfer between molecules. To confirm this hypothesis theoretical calculations that are outside of the scope of the present work would be required. On the contrary, the presence of isolated and aggregated molecules forming disordered clusters (see Figure 8 and S11, Supporting Information) indicates that the growth of a well-ordered $C_{60}F_{18}$ layer on the CORO monolayer, which would somehow mimic the D/A interface of a given co-crystal, is hindered at the growth conditions employed.

As an alternative to the two-step sequential evaporation of donor and acceptor, the co-evaporation of CORO and $C_{60}F_{18}$ was also tested. However, instead of a mixed compound, affinity

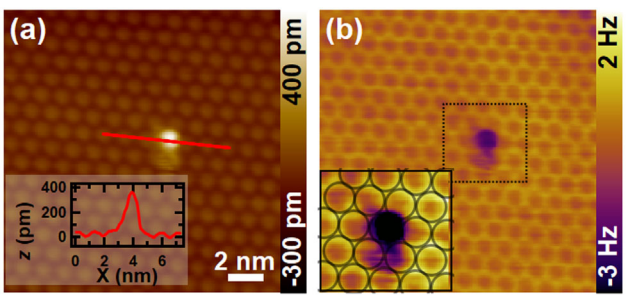

Figure 9. Topographic (a) and frequency shift (b) images of a single $C_{60}F_{18}$ deposited on a monolayer of CORO/Au(111). The inset in (a) shows a cross section along the red line. The inset in (b) is a magnification of the square marked with a dashed line. In the inset, the CORO lattice has been superimposed with circles.

for direct adsorption on Au(111) compels CORO to form the ordered flat monolayer, therefore, leading to similar results (see Figure S12, Supporting Information). Because both electronic and steric effects come into play in the co-crystal formation, we believe that the molecular tilt of the CORO molecules with respect to the plane, defined by their centroids, plays a crucial role. As determined from X-ray diffraction, due to the tilt of CORO in the co-crystal there is no aromatic π–π overlap between the CORO donor and the $C_{60}F_{18}$ acceptor, and the in-plane periodicity of CORO in the co-crystal (shorter than that of CORO on the surface) imposes a constrained orientation of the $C_{60}F_{18}$ dipoles. Conversely, when adsorbed on the metal surface, the interaction between the π-electrons of CORO and the high density of gold surface states forces the molecule to adopt a planar adsorption geometry, overall influencing the subsequent $C_{60}F_{18}$ dipole accommodation. In other words, the flat orientation of CORO facilitates the π−π interaction between $C_{60}F_{18}$ and CORO (see Figure 9b). We suggest that choosing a different substrate with a weaker CORO-surface interaction or allowing the formation of CORO multilayers could be advantageous to modulate the relative orientation of molecules by means of CORO tilted phases.[38,39] Unfortunately, growing predesigned heterostructures in UHV presents significant challenges. In this regard, deposition from a mixed solution of $C_{60}F_{18}$ and CORO could have the advantage of being closer to equilibrium conditions, although this could lead to incorporation of the solvent into the assembly, which is a common observation with PAHs. Moreover, other parameters would come into play, such as the optimal molecular ratio in solution required to achieve the desired stoichiometry of the on-surface $C_{60}F_{18}$/CORO co-crystals (see above).

3. Conclusion

This work provides the structure of a series of donor-acceptor complexes formed by the combination of the fluorofullerene acceptor $C_{60}F_{18}$ with three PAH donors varying in size, from the four fused ring system of PYRN to the large seven fused ring system of CORO. Each of the three structures has a different D:A stoichiometric ratio, and a variability in the co-crystal packing structure. Most interesting is the apparent relationship between the donor PAH size and packing. In combination with PYRN, the smallest PAH donor used, the resulting co-crystal has a complex mixed packing of $C_{60}F_{18}$ and PYRN molecules, allowing three PYRN molecules to have π–π interactions with a single $C_{60}F_{18}$ molecule. In the structure $(PYRN)_2/C_{60}F_{18}{\cdot}CH_2Cl_2$, the PYRN molecules do not interact, suggesting that the co-crystal formation is driven by the maximization of the interactions between D and A molecules. This strong affinity between PYRN and $C_{60}F_{18}$ is believed to be responsible for the long retention time for $C_{60}F_{18}$ on the PYRN based stationary phase of the Buckyprep chromatographic column. In contrast, for the larger PAHs, PERY, and CORO, donor and acceptor molecules pack alternately in layers with a segregated packing mode, D/A/D/A for PERY and D/A/A/D/A/A for CORO. For CORO/$(C_{60}F_{18})_2$, the electric dipole of $C_{60}F_{18}$ molecules are all aligned in the double layer, with an opposite alignment in alternate bilayers. The observed variations in the packing motifs

of the three systems are likely caused by the combination of steric and electronic effects.

In an attempt to obtain on-surface supported co-crystals and mimic the D/A interface of the co-crystal, we have investigated the assembly of $C_{60}F_{18}$ and CORO deposited from evaporation on Au(111) in UHV using STM. Our study confirms the capability of forming high-quality CORO monolayers as well as determining the adsorption of single $C_{60}F_{18}$ molecules at the center ring of CORO. This is a promising result to access molecule–molecule charge transfer in D/A complexes. Unfortunately, no ordered architectures of CORO and $C_{60}F_{18}$ have been obtained so far through sequential deposition of $C_{60}F_{18}$ on CORO or by co-evaporation. Whether this goal can be achieved, further efforts are needed to explore alternative approaches. In this context, while surface engineering (changing or modifying the substrate to reduce its influence) or solution processing methods can be useful, the dominant steric and electronic effects in co-crystals require combining local STM characterization with precise theoretical calculations/simulations.

Overall, this work provides a rare opportunity to investigate intermolecular interactions of a spheroidal electron acceptor with planar electron donors, which may extend to other D/A systems with similar structures that have, besides fundamental interest, a practical importance in optoelectronic devices involving charge- and energy-transfer.

4. Experimental Section

Materials

The following compounds were obtained from the indicated supplier and were used as received: CORO (TCI America, 95.0%), PERY (Sigma-Aldrich, 99%), PYRN (Alfa Aesar, 98%), C_{60} (MTR Ltd., 99.5%), and DCM (Fisher Scientific, ACS grade) were used as received. A sample of $C_{60}F_{18}$ was synthesized as described previously.[23] A crude reaction product contained small impurities of unreacted C_{60} and fluorofullerenes $C_{60}F_n$, where $n < 18$ and it was subjected to further purification by HPLC using Cosmosil BuckyPrep column (Nackalai Tesque, Japan) in 100% toluene at 5 mL min^{-1} flow rate (370 nm wavelength detection). The purity of the $C_{60}F_{18}$ sample was estimated as 90%+, based on HPLC and ^{19}F NMR data.

X-ray Crystallography for PAH/$C_{60}F_{18}$

Crystals of PAH/$C_{60}F_{18}$ CT complexes suitable for diffraction were grown by slow evaporation of DCM solutions under ambient conditions. Diffraction data were collected at the Advanced Photon Source at Argonne National Laboratory on beamline 15ID-D, using a diamond 111 monochromator, an X-ray wavelength of 0.41328 Å, a Bruker D8 goniometer, and multi-scan absorption corrections. Unit cell parameters were determined by the least squares fit of the angular coordinates of all reflections. Integrations of all frames were performed using APEX III software, and the structures were solved using SHELXTL/OLEX 2 software. Crystallographic data collection and final refinement parameters for all three structures are listed in Table 1.

The CORO/$(C_{60}F_{18})_2$ CT/CC structure was rotationally disordered about two CORO positions. In order to model the presumed two-part disorder, ISOR and SAME commands were used to build the second half-coronene moiety. A large residual electron density of 1.8 e^- $Å^{-3}$ appears in the structure, likely resulting from a disordered DCM molecule occupying space between the fullerenes. Unfortunately, the SQUEEZE function was not able to remove this residual electron density, apparently due to its close proximity between the two fullerenes. The $(PYRN)_2/C_{60}F_{18}$ crystal has an inversion twin that was modeled using the inversion twin law with a BASF value of 0.32. The CT/CC structure of PERY/$C_{60}F_{18}$ differs from the other two in that it is a 1:1 donor/acceptor structure and exhibited no disorder.

UV-Vis Spectroscopy of PAH/$C_{60}F_{18}$

UV-vis spectra for the PAH/$C_{60}F_{18}$ CT complexes in dichloromethane were recorded using an Agilent 8453 UV-visible spectrophotometer.

STM Measurements

The STM measurements were performed at RT using a commercial Aarhus SPM 150 with KolibriSensor sensors ($f \approx 1$ MHz, $Q \approx 25{,}000.00$) and a Nanonis Control System (SPECS Surface Nano Analysis GmbH). The sharp metallic tip was cleaned in situ via Ar^+ sputtering and, during STM measurements, was maintained oscillating at a constant amplitude ($A = 200$ pm). Topographic STM was conducted in the constant current mode ($I = cte$) and the simultaneous frequency shift was recorded. Typical tunneling parameters were sample bias voltages (U) of 1–2 V and currents (I) of 100–200 pA. The in-plane lattice constant, in high-resolution images, and step heights, in large-scale images of the clean Au(111) were employed for calibration of the STM piezo scanner. Au(111)/mica were cleaned in UHV by cycles of argon etching (500 eV) and annealing at 320 °C. Molecules were deposited from sublimation under UHV and the samples were transferred in situ to the STM. The molecular coverage was estimated directly from the topographic STM images. For CORO a complete monolayer was observed after an exposure of 5 min (sublimation temperature 180 °C). For $C_{60}F_{18}$ and regardless of the exposure time (sublimation temperature of 190 °C), it was not possible to obtain a complete and flat monolayer. In Figure 7 and 8 the exposure time was 5 min.

Acknowledgements

The authors thank the National Science Foundation (grant NSF/CHE-2153922) (S.B., O.V.B.), the Office of Basic Energy Sciences, and the Colorado State University Research Foundation for partial financial support. NSF's ChemMatCARS Sector 15 is principally supported by the National Science Foundation under grant nos. NSF/CHE-1834750 and NSF/CHE-2335833. Use of the Advanced Photon Source was supported by the U.S. Department of Energy, Office of Science, and Office of Basic Energy Sciences under Contract DE-AC02-06CH11357. Part of the experimental work is based on doctoral theses of Dr. N.D.[40] and Dr. L.K.S.[41] Dr. D.M.-J. acknowledges funding from European Union under the Horizon Europe Marie Sklodowska-Curie Actions (project TORNADE, g. a. no. MSCA-PF-101106103). This work was partially funded by the Spanish Ministry of Science and Innovation (MCIN) and State Investigation Agency (AEI) under Project PID2022-136802NB-I00 (AEI/FEDER, UE) and through the Severo Ochoa Programme for Centers of Excellence in R&D (grant CEX2023-001263-S). This study is part of the Spanish Advanced Materials Programme (Project IN-CAEM) supported by the MCIN with funding from European Union NextGenerationEU (grant PRTRC17.I1) and by Generalitat de Catalunya.

Conflict of Interest

The authors declare no conflict of interest.

Data Availability Statement

The data that support the findings of this study are available from the corresponding author upon reasonable request.

Keywords: donor–acceptor interactions · fluorofullerenes · layered stacking · polycyclic aromatic hydrocarbons · scanning tunneling microscopy

[1] T. Kawase, *Chem. Nanocarb.* **2010**, 189.
[2] C. Cui, Y. Li, Y. Li, *Adv. Energy Mater.* **2017**, *7*, 1601251.
[3] A. J. Ferguson, J. L. Blackburn, N. Kopidakis, *Mater. Lett.* **2013**, *90*, 115.
[4] C. García-Simón, M. Costas, X. Ribas, *Chem. Soc. Rev.* **2016**, *45*, 40.
[5] A. S. Oshchepkov, *ChemPhysChem* **2024**, *25*, e202400435.
[6] J. Ristein, *J. Phys. D: Appl. Phys.* **2006**, *39*, R71.
[7] B. Lussem, C.-M. Keum, D. Kasemann, B. Naab, Z. Bao, K. Leo, *Chem. Rev.* **2016**, *116*, 13714.
[8] I. Salzmann, G. Heimel, M. Oehzelt, S. Winkler, N. Koch, *Acc. Chem. Res.* **2016**, *49*, 370.
[9] A. A. Dar, S. Rashid, *CrystEngComm* **2021**, *23*, 8007.
[10] K. P. Goetz, D. Vermeulen, M. E. Payne, C. Kloc, L. E. McNeil, O. D. Jurchescu, *J. Mater. Chem. C* **2014**, *2*, 3065.
[11] L. Sun, Y. Wang, F. Yang, X. Zhang, W. Hu, *Adv. Mater.* **2019**, *31*, 1902328.
[12] O. Boltalina, in *New Fluorinated Carbons: Fundamentals and Applications* (Eds: O. Boltalina, T. Nakajima), Elsevier, Amsterdam, Netherlands **2017**, pp. 1–34.
[13] I. S. Neretin, K. A. Lyssenko, A. Y. Antipan, Y. L. Slovokhotov, O. V. Boltalina, P. A. Troshin, A. Y. Lukonin, L. N. Sidorov, R. Taylor, *Angew. Chem Int. Ed.* **2000**, *39*, 3273.
[14] C. B. Hübschle, S. Scheins, M. Weber, P. Luger, A. Wagner, T. Koritsánszky, S. I. Troyanov, O. V. Boltalina, I. V. Goldt, *Chem. Eur. J.* **2007**, *13*, 1910.
[15] J. Poater, X. Fradera, M. Duran, M. Sola, *Chem. Eur. J.* **2003**, *9*, 1113.
[16] O. V. Boltalina, S. H. Strauss, in *Dekker Encyclopedia of Nanoscience and Nanotechnology* (Eds: J. A. Schwarz, C. Contescu, K. Petyera), Marcel Dekker, New York **2004**, pp. 1175–1190.
[17] *NIST Chemistry WebBook*, NIST Standard Reference Database Number 69 (Eds: P. J. Linstrom, W. G. Mallard), National Institute of Standards and Technology, Gaithersburg, MD **2024**, https://webbook.nist.gov/chemistry/.
[18] J. W. Hager, S. C. Wallace, *Anal. Chem.* **1988**, *60*, 5.
[19] S. Kumar, Y. T. Tao, *Chem. Asian J.* **2021**, *16*, 621.
[20] X.-Y. Wang, X. Yao, K. Müllen, *Sci. China Chem.* **2019**, *62*, 1099.
[21] O. Boltalina, in *The Curious World of Fluorinated Molecules: Molecules Containing Fluorine*, Vol. *6* (Ed: K. Seppelt), Elsevier, Amsterdam, Netherlands **2020**.
[22] X.-B. Wang, C. Chi, M. Zhou, I. V. Kuvychko, K. Seppelt, A. A. Popov, S. H. Strauss, O. V. Boltalina, L.-S. Wang, *J. Phys. Chem. A* **2010**, *114*, 1756.
[23] O. V. Boltalina, V. Y. Markov, R. Taylor, M. P. Waugh, *Chem. Commun.* **1996**, 2549.
[24] O. V. Boltalina, J. M. Street, R. Taylor, *J. Chem. Soc., Perkin Trans. 2* **1998**, 649.
[25] I. V. Kuvychko, A. V. Streletskii, N. B. Shustova, K. Seppelt, T. Drewello, A. A. Popov, S. H. Strauss, O. V. Boltalina, *J. Am. Chem. Soc.* **2010**, *132*, 6443.
[26] E. V. Bukovsky, B. W. Larson, T. T. Clikeman, Y.-S. Chen, A. A. Popov, O. V. Boltalina, S. H. Strauss, *J. Fluorine Chem.* **2016**, *185*, 103.
[27] R. Taylor, A. K. Abdul-Sada, O. V. Boltalina, J. M. Street, in *Recent Advances in the Chemistry and Physics of Fullerenes and Related Materials: Proc. of the Twelfth [sic] Int. Symp.*, Vol. *99*, Electrochemical Society, Pennington, NJ **1999**, p. 188.
[28] X. Bouju, C. Mattioli, G. Franc, A. Pujol, A. Gourdon, *Chem. Rev.* **2017**, *117*, 1407.
[29] N. W. Kabat, E. Monazami, P. Reinke, *PCCP* **2020**, *22*, 26972.
[30] B. Chilukuri, U. Mazur, K. Hipps, *PhysChemChemPhys* **2019**, *21*, 10505.
[31] A. Jahanbekam, S. Vorpahl, U. Mazur, K. Hipps, *J. Phys. Chem. C* **2013**, *117*, 2914.
[32] C. Seidel, R. Ellerbrake, L. Gross, H. Fuchs, *Phys. Rev. B* **2001**, *64*, 195418.
[33] E. Goiri, P. Borghetti, A. El-Sayed, J. E. Ortega, D. G. de Oteyza, *Adv. Mater.* **2016**, *28*, 1340.
[34] R. Palacios-Rivera, D. C. Malaspina, N. Tessler, O. Solomeshch, J. Faraudo, E. Barrena, C. Ocal, *Nanoscale Adv.* **2020**, *2*, 4529.
[35] T. K. Shimizu, J. Jung, T. Otani, Y.-K. Han, M. Kawai, Y. Kim, *ACS Nano* **2012**, *6*, 2679.
[36] S. I. Oreshkin, M. N. Petukhov, D. A. Muzychenko, V. I. Panov, V. O. Surov, A. V. Samorodskii, A. I. Oreshkin, *JETP Lett.* **2024**, *119*, 211.
[37] K. Bairagi, A. Bellec, R. G. Chumakov, K. A. Menshikov, J. Lagoute, C. Chacon, Y. Girard, S. Rousset, V. Repain, A. M. Lebedev, L. P. Sukhanov, N. Y. Svechnikov, V. G. Stankevich, *Surf. Sci.* **2015**, *641*, 248.
[38] C. Xu, Y. Que, Y. Zhuang, Z. Lin, X. Wu, K. Wang, X. Xiao, *J. Phys. Chem. B* **2018**, *122*, 601.
[39] J. Martinez-Blanco, A. Mascaraque, Y. S. Dedkov, K. Horn, *Langmuir* **2012**, *28*, 3840.
[40] N. J. DeWeerd, *Ph.D. Thesis*, Colorado State University, USA **2020**.
[41] L. K. San, *Ph.D. Thesis*, Colorado State University, USA **2015**.

Manuscript received: March 31, 2025
Revised manuscript received: May 21, 2025
Version of record online: